

Lipid Bilayer Membrane Perturbation by Embedded Nanopores: a Simulation Study

Rebeca Garcia-Fandiño^{1,3}, Angel Piñeiro², Jemma Trick³ and Mark S. P. Sansom^{3*}*

¹Center for Research in Biological Chemistry and Molecular Materials (CIQUS),
University of Santiago de Compostela, Spain.

²Soft Matter & Molecular Biophysics Group, Department of Applied Physics, Faculty
of Physics, University of Santiago de Compostela, Spain.

³Department of Biochemistry, University of Oxford, South Parks Road, Oxford OX1
3QU, United Kingdom.

*To whom correspondence should be addressed.

E-mail: rebeca.garcia.fandino@usc.es & mark.sansom@bioch.ox.ac.uk

ABSTRACT:

A macromolecular nanopore inserted into a membrane may perturb the dynamic organization of the surrounding lipid bilayer. To better understand the nature of such perturbations, we have undertaken a systematic molecular dynamics simulation study of lipid bilayer structure and dynamics around three different classes of nanopore: a carbon nanotube, three related cyclic peptide nanotubes differing in the nature of their external surfaces, and a model of a β -barrel nanopore protein. Periodic spatial distributions of several lipid properties as a function of distance from the nanopore were observed. This was especially clear for the carbon nanotube system, for which the density of lipids, the bilayer thickness, the projection of lipid head-to-tail vectors onto the membrane plane, and lipid lateral diffusion coefficients exhibited undulatory behaviour as a function of the distance from the surface of the channel. Overall, the differences in lipid behaviour as a function of the nanopore structure reveal local adaptation of the bilayer structure and dynamics to different embedded nanopore structures. Both the local structure and dynamic behaviour of lipids around membrane-embedded nanopores are sensitive to the geometry and nature of the outer surface of the macromolecule/ molecular assembly forming the pore.

Keywords: nanopores; lipid bilayer; carbon nanotube; cyclic peptide nanotubes; β -barrel nanopore protein

Biological membranes separate the contents of a cell from its environment and/or form compartments within cells. These membranes are formed of a lipid bilayer, in which are embedded different classes of integral membrane proteins which enable and control transport of molecules across the membrane. Two major classes of membrane proteins, namely ion channels and bacterial porins, form nanoscale pores within membranes. These biological nanopores combine selectivity for the species which may pass through them with high (*i.e.* near diffusion limited) rates of solute permeation. The selectivity and efficiency of these biological nanopores has stimulated the design of simpler models which mimic natural systems whilst offering the possibility of developing novel functions and properties.¹⁻⁴ The development of such biomimetic materials will contribute to develop bioinspired smart nanopore devices that may be employed for stochastic biosensors, selective water pores for desalination, and for biomedical diagnostics.³ A number of different materials have been used to form biomimetic nanopores in lipid bilayers, including carbon nanotubes (*e.g.* CNT porins,⁵ self-assembled cyclic peptide nanotubes,^{2, 6-9} and nanotubes formed by DNA origami¹⁰). If such biomimetic nanopores are intended to be used in stable membranes within nanodevices it is important that we understand the relationship between their structure and the possible perturbation of the properties of the surrounding lipid bilayer.

Lipids may be considered as the ‘solvent molecules’ for membrane embedded macromolecules. As for water molecules around a protein in aqueous solution,¹¹⁻¹⁴ three classes of lipids may be considered as a function of the strength of their interaction with membrane proteins (Figure 1).^{15, 16} Lipid molecules with a low degree of interaction with the protein transmembrane domain may be considered as “bulk” lipids. Lipid interactions with a nanopore may be affected by the specific interactions between the nanopore and the lipid head polar groups, by hydrophobic (mis)matching of the nanopore and the hydrocarbon chains of the lipids, or both. Such interactions may lead to a significant reduction of exchange rates with the “bulk” lipids and, consequently, to the formation of a lipid annulus surrounding the membrane protein. Lipids with even lower exchange rates are sometimes referred to as non-annular lipids and in the case of membrane proteins they often interact with specific binding sites on the surface of the protein.¹⁶

- **Figure 1 here:**

Biochemical and biophysical studies have demonstrated the importance of protein–lipid interactions in membrane structure and function^{15, 17}, and have also allowed the dynamics of lipids within such membranes to be probed. *In silico* approaches play a key role in enabling us to analyse nanopore/protein-lipid interactions and dynamics at atomic resolution.^{18, 19} Molecular dynamics (MD) simulations provide a dynamic view of such systems, and also a useful framework to aid interpretation of experimental results.^{20, 21} MD simulations have shown that the effects of a membrane protein inserted into a lipid bilayer are generally restricted to the few layers of lipids immediately around the protein,²² in agreement with the scheme proposed in Figure 1. For example, MD simulations of the peptide channel/nanopore gramicidin A embedded in dimyristoylphosphatidylcholine [di(C14:0)PC] bilayer showed that it was possible to distinguish between lipid molecules next to the channel (*i.e.* phospholipids that were either hydrogen bonded directly to the channel or *via* one intervening water molecule) and the ‘bulk’ lipid which is not hydrogen bonded to the channel.²³ Interactions of the lipid bilayer with ion channels also play a key role in voltage activation of Kv and related ion channels²⁴⁻²⁶. Studies carried out on the interactions between membrane proteins and lipids could be extrapolated in some extent to other macromolecular nanopores embedded in the bilayer. Thus, an analogous behavior of the lipids has been suggested from single or multiple wall carbon nanotubes (SWCNTs or MWCNTs) embedded into a model membrane, using coarse-grained MD simulations.²⁷

In the present work, a systematic atomic resolution MD study of the structure and dynamics of DOPC (1,2-Dioleoyl-sn-glycero-3-phosphocholine) molecules around different heterogeneous structures including a β -barrel nanopore, a SWCNT, and three different species of nanotube formed by cyclic peptides inserted into a lipid membrane is performed. This study reveals the effects of different pore structures and their outer surfaces on the perturbation of the dynamic organization of the surrounding lipids. A detailed understanding of the effects of inserted nanoparticles on biomembrane structure and dynamics is crucial for the design of stable biomimetic nanopores and for the reduction of possible cytotoxic side-effects.²⁸

RESULTS AND DISCUSSION

Models. In order to explore the relationship between the nanopore surface and their interactions with a phospholipid bilayer, three classes of nanopore models were explored: a (single walled) carbon nanotube (CNT); self-assembled cyclic peptide nanotubes (SCPNS); and a simple model of a β -barrel membrane protein nanopore (Figure 2). Each nanopore structure was embedded in a lipid bilayer (formed by the phospholipid DOPC), solvated with 1 M NaCl aqueous solution, and simulated atomistically for 30 ns.

- **Figure 2 here:**

CNT. An armchair (14,14) carbon nanotube was modelled with four carboxylate groups attached to its inner wall, in the central region of the channel (Figure 2A).²⁹ CNTs have unique properties which suggest a number of possible applications in biomedicine.³⁰ Several studies have indicated that CNTs can be spontaneously inserted into lipid membrane bilayers.⁵ Additionally, the insertion of intercalated carbon nanotubes on lipid bilayers has proved to “strengthen” ambient lipids and it prevents the whole system from further destabilization by high temperatures.³¹

Self-assembled Cyclic Peptide Nanotubes. SCPNs are cyclic peptide (CP) structures that adopt a planar conformation with the amide groups arranged perpendicularly to the plane.³² Thus, the cyclic peptide may be stacked to form extended nanopore β -sheets. The sidechains of the cyclic peptides point outwards from the nanotube surface, and thus by changing the sidechains one may modulate the formation and properties of SCPNs. It has been shown that, depending on the peptide sequence, the SCPNs may be oriented perpendicularly^{9, 33, 34} to the bilayer (hydrophobic CPs) or parallel to the bilayer plane³⁵. In the current work we have explored study the effect of three different SCPNs (**SCPNA_{Ala}**, **SCPNL_{Leu}**, **SCPNT_{Trp}**; Figure 2B-D) which are oriented perpendicular to the bilayer plane. The constituent CPs are composed of (1R,3S)-3-aminocyclohexanecarboxylic acid (D- γ -Ach) combined with α -amino acids of appropriate chirality (Ala, Leu or Trp, respectively).^{36, 37} Thus the external surface is covered with either small hydrophobic sidechains (**SCPNA_{Ala}**), bulky hydrophobic sidechains (**SCPNL_{Leu}**), or large aromatic sidechains (**SCPNT_{Trp}**). We note that in **SCPNT_{Trp}** the Trp side chains are capable of hydrogen bonding to lipid headgroups, and thus they mimic the bands of Trp sidechains which are often found on the surface of

membrane proteins, and which are thought to help stabilize such proteins in their correct location in a lipid bilayer.³⁸

β-barrel nanopore. A simple minimalist model of a biomimetic β-barrel nanopore (**β-barrel**) was generated, in which the outer surface was covered with hydrophobic Leu side chains with a band of Trp sidechains at either end of the nanotube (Figure 2E).³⁹ This structure is expected to be stable when embedded in a lipid bilayer, and indeed has been shown to remain stably embedded in a PC bilayer during multiple simulations of up to 100 ns duration.³⁹

Lipid density around the nanopores. Given the differences in smoothness, hydrophobicity, and hydrogen bonding potential between the three classes of nanopore, one might anticipate differences in the distribution of lipids around them, and in particular in the formation of rings of annular lipids. This can be explored by calculation of radial distribution functions (RDFs) of lipid tails and of lipid headgroups around the nanopores (Figure 3). From this analysis two clear trends emerge: the first is that the RDFs for the lipid tails indicate the formation of concentric shells around the nanotubes, but that this is much less evident for the lipid head groups. The second trend is in terms of the degree of structuring of the lipid tails into concentric shells decreases as the nanotube becomes less ideally cylindrical, in the order $\text{CNT} > \text{SCP}_{\text{NAla}} > \text{SCP}_{\text{NLeu}} \approx \text{SCP}_{\text{NTrp}} \approx \text{β-barrel}$. Thus the interaction between the smooth hydrophobic surface of the CNT and the polar heads of DOPC molecules is not favourable, whereas the hydrophobic lipid tails clearly form a tight first layer around the pore in direct contact with the CNT structure.⁴⁰ Lipids are also arranged in successive concentric layers around the immediate annular layer for this nanopore, with decreasing density as the distance from the nanopore increases. Beyond three or four layers, the lipids gradually ‘lose memory’ of the CNT surface and distribute randomly as in a bulk membrane. The RDF of the headgroups does not show such a clear trend probably due to their higher mobility and their lack of strong interactions with the hydrophobic surface of the CNT.

- ***Figure 3 here:***

For the simulations with SCPNs embedded in the bilayer, the peaks in the RDF are not as well defined as for the CNT, although the spacing between the first and successive peaks are similar (for *e.g.* SCP_{NAla} and for the CNT) suggesting that overall concentric

shells of lipids are formed. A more detailed examination of average lipid densities in the plane of the bilayer around each class of nanotube (Figure 4) reveals that for the smooth CNT, rotationally symmetric rings of lipid density are seen. For **SPCN_{Ala}** the first ring of lipids is largely retained whereas for the other nanopores (which deviate more markedly from circular rotational symmetry, *i.e.* are less ideally cylindrical in structure) this is not the case. Furthermore, the subsequent concentric undulations are not as clear as with CNT for all of the other nanopore systems. This is also evident from the relative amplitudes of the RDF of the lipid tails (Figure 3) which are significantly lower for the other systems (especially for **SCPN_{Leu}** and **SCPN_{Trp}**) than they are for the **CNT** system.

- **Figure 4 here:**

Bilayer thickness. The thickness of a lipid bilayer may be defined as the distance between opposing head groups of the two leaflets. For the DOPC bilayer the mass density profile along the bilayer normal (z axis) gives a hydrophobic thickness of ca. 3.6 nm. Insertion of the nanopores causes some local thinning of the DOPC bilayer (SI Figure S3). 2D density maps projected in the YZ plane (calculated using the program *g_lomepro*,⁴¹; Figure 5 and SI Figure S1b) suggest that there is some thinning of the membrane local to the nanopore along with a degree of thickening at intermediate distances. This is clearest for the **CNT** system, less so for the other nanopores (SI Figure S2), and has been attributed to the tilting of the lipid tails away from the nanopore.⁴²

- **Figure 5 here:**

Lipid order parameters. The headgroup dipoles of PC lipids tend to lie nearly parallel to the bilayer plane.⁴³ It has also been observed that phospholipid head groups may adjust their orientation to optimize their interaction with water in proximity to carbon nanopores.⁴⁴ The lipid tails are more flexible but on average they tend to be oriented parallel to the bilayer normal. The distribution of the lipid head-to-tail vectors projected onto the membrane plane and averaged over the last 20 ns of the nanopore simulations have been calculated (Figure 6 and SI Figures S4-S8) to characterize possible lipid ordering around the nanopores. For the CNT nanopore the orientations of the lipid chains again reveal very clear concentric layers around the CNT channel

characterized the radial and tangential component of the vectors. Thus the CNT has a strong effect on the local ordering of the lipids. Remarkably, the two tails of DOPC exhibit a different behaviour between each other in the first layer. The tangential component of the *sn2* lipid tail is much larger than that of the *sn1* tail. This phenomenon can be rationalized on the basis of the known conformational differences between the *sn1* and *sn2* fatty acyl chains of glycerolipids. The acyl chain at position 2 begins roughly parallel to the bilayer surface before bending at the C2 to orient the hydrocarbon chain perpendicular to the bilayer plane, whereas the fatty acyl chain at position 1 is perpendicular to the bilayer throughout its entire length.⁴⁵ Additionally, the orientation of the *sn1* tail in the first layer is clearly clockwise for both leaflets (Figure 6A and SI Figure S4). The comparison between leaflets for this system is also interesting. The major difference is the size of the radial component corresponding to the *sn1* tail in the first layer around the nanopore, which is considerably larger in the leaflet with lower number of lipids (note that the distribution of lipids is not equivalent between leaflets). This is extremely interesting since it could shed light on adaptation mechanisms of lipid membranes to fit macromolecular structures. The dependence of the lipid tail orientation with the distance to the nanopore is clear. In general, the size of the vectors becomes lower as the distance increases, as a result of the increasing random orientation in the same direction and the subsequent cancellation of compounds upon averaging.

- **Figure 6 here:**

The behaviours of the other nanopore systems in terms of lipid ordering are very different from those for the CNT. Concentric ordered rings are not seen, but rather there is some evidence for (nano)domains of lipid in both leaflets of the bilayer for the membranes containing either SCPNs and or the β -barrel model. Thus the more irregular and less hydrophobic surfaces of these nanopores result in absence of marked local ordering of the lipid orientations around the nanopore.

Lipid diffusion. A number of simulation studies of membrane proteins have suggested that lipids associated with the protein diffuse more slowly than bulk lipids in both atomistic⁴⁶ and in coarse-grained simulations²². Indeed, the major distinction between annular and “bulk” lipids has been attributed to their exchange rates at the

nanopore-lipid interface. It is therefore worth to explore to what extent the different surfaces of the three classes of nanopore influence the diffusion of lipids in the bilayer in which the nanotubes are embedded. In the current study the effect of the nanopore on the lipid diffusion rate as a function of distance from the nanopore is relatively small, perhaps reflecting weaker interactions of the nanopores with their lipid bilayer environment (Figure 7, Figures S9-S11). Interestingly there are some suggestions of spatial periodicity for lipid diffusion rates, especially for the **CNT** system. This is likely to reflect the effect of the concentric shells of lipid discussed above on the dynamics of lipid diffusion. For some of the systems (*e.g.* **SCPN_{Ala}**, **SPCN_{Leu}**) there is a small increase of the *D* close to the surface of the nanotube for low Δt values ($\Delta t=0.1$ ns, Figure S12). This suggests for the first time that those lipids near the surface of these nanotubes may experience a ballistic motion diffusion regime, analogous to what is seen for *e.g.* confined water molecules near the inner walls of a CNT.^{47, 48}

- **Figure 7 here:**

Lipid hydrogen bonding to nanopores. The **SCPN_{Trp}** and **β -barrel** nanopores have multiple tryptophan sidechains on their surfaces, capable of forming hydrogen bonds (H-bonds) to lipid headgroups. Analysis of the number of H-bonds along the simulation trajectories suggests that up to 7 or 9 H-bonds are formed between these nanopores and the lipids (Figure 8). Thus these two classes on nanopores resemble integral membrane proteins which are often ‘locked’ into a lipid bilayer *via* the formation of H-bonds between Trp sidechains of the protein and lipid headgroups.

In the **CNT**, **SCPN_{Ala}**, **SPCN_{Leu}** systems the analysis of lipid diffusion at $\Delta t=0.1$ ns (SI Figure S12) suggests possible sub-diffusive or ballistic diffusion of the lipids near the walls of these smoother nanopores which cannot form H-bonds to lipid headgroups. This suggests that the lipids near the nanotube walls may experience a ballistic motion diffusion regime. The absence of this effect in those systems with a rougher surface, such as **SCPN_{Trp}** or the **β -barrel**, may be related to the ability of these nanopores to form H-bonds with nearby lipids.

- **Figure 8 here:**

Possible functional implications. It is of interest to consider whether the ring-like local organization of lipids around the nanopores is reflected in the local organization of water and ions, with possible consequent functional implications for permeation of nanopores by water and/or ions. This may be addressed by calculation of radial distribution functions for water and for ions in the plane of the bilayer around the nanopores (see Fig. 9). This analysis reveals two aspects. Firstly, water and ion densities (as reflected in the RDFs) *within* the pores as a function of distance from the centre of the pore. To some extent this has already been discussed in previous studies^{29, 37} Secondly, water and ion RDFs in the plane of the bilayer for distances corresponding to *outside* the nanopores reveal any local ordering of the electrolyte solution in the vicinity of the nanopore as a consequence of the distribution of lipids.

Around the pores ‘ripples’ in the $g(r)$ for Na^+ ions can be seen, extending out as far as r ca. 3 nm. These ‘ripples’ are reminiscent of the $g(r)$ curves for lipids (Fig. 3) and suggest a degree of local organization of the electrolyte solution at the bilayer surface around the nanopores as a consequence of the local (annular) organization of lipids. This is in agreement with simulation studies of the interactions of alkali cations and halides around the lipid headgroups of a DOPC bilayer^{49, 50} We suggest that this local ordering of the sodium ions may have functional consequences, as access of ions to the mouth of the nanopores is in part mediated by an electrolyte solution which is more ‘structured’ than in the bulk solution. This effect might be anticipated to be more marked with different (*e.g.* anionic) lipids⁵¹, and with different species of ions⁵², and indeed this could be an interesting topic for future studies.

- **Figure 9 here:**

CONCLUSION

A systematic simulation study on the lipid structure and dynamics around several classes of nanopore has been performed. Periodic spatial distributions of several properties, corresponding to concentric rings of locally ‘perturbed’ lipids, were observed. This behaviour was especially clear for the CNT nanotube. In contrast, the behaviour of the lipid molecules around the protein-like β -barrel nanopore seemed to be less ordered, and concentric rings of perturbed lipids were not observed. The

nanopores formed by SCPNs were intermediate in their behaviour, with the simpler **SCPNA_{Ala}** nanopores being more similar to CNTs, whilst the more complex **SCPNT_{Trp}** nanopores more closely resembled the **β -barrel**. This suggests a general relationship between how hydrophobic and smooth a nanopore is and the extent to which the bilayer is locally perturbed. The rougher surfaces, also capable of forming H-bonds, of the **SCPNT_{Trp}** and **β -barrel** nanopores seem to cause less local perturbation of the surrounding lipids.

Significantly, the **CNT** nanopore generates the greatest perturbations of the membrane, and it is perhaps the most toxic of the nanopores evaluated.⁵³ This suggests that to generate a nanopore which will insert into a membrane without perturbing the structure and dynamics of a membrane, one should design the outer surface to mimic that of a native membrane protein. The **SCPNT_{Trp}** and the **β -barrel** nanopores represent the first steps of designing such features into a nanopore. Recent advances in re-designing *e.g.* bacterial outer membrane proteins⁵⁴ may aid in further refinement of such designs. In particular, it would be interesting to explore ‘hybrid’ SCPN nanotubes with *e.g.* a central core of **SCPNL_{Leu}** molecules with **SCPNT_{Trp}** molecules at either end of the nanotube to facilitate stabilising interactions with lipid headgroups.

Overall, the large differences observed for the lipid behaviour as a function of the nanopore structure reveal adaptation mechanisms of membranes to host different structures. Both the local structure and dynamic behaviour of lipids around membrane-embedded nanopores are revealed to be sensitive to the nature of the embedded macromolecule or molecular assembly. This may be of more general relevance in terms of mechanosensitivity (*e.g.* stretch activation) mediated by nanopore-lipid interactions, which is seen in biological pores such as potassium channels^{24, 55, 56} and bacterial mechanosensitive channels⁵⁷ and has been suggested for *e.g.* synthetic nanopores formed by DNA origami⁵⁸.

METHODS:

Molecular dynamics simulation parameters. The coordinates and parameters for the **CNT** model were obtained from previous studies.²⁹ For the SCPNs, RESP/6-31G(d) charges were derived as in the original AMBER force-field development, while van der Waals parameters were taken from the GAFF force-field⁵⁹ using standard Lorenz–Bertelot combination rules.^{36, 37} The **β -barrel** model structure was from a

previous study⁴⁸ and parameters from the AMBER⁶⁰ force field. The water (SPC/E)/ion combination parameters published by Joung et al.,⁶¹ as implemented in AMBER were used. The GAFF⁶² force field was used for DOPC as in previous studies⁶³ from which we obtained a pre-equilibrated bilayer. The bilayer was replicated three times in the x and y directions and, after nanopore insertion, the complete system was solvated. Water molecules in the hydrophobic region of the tails and also inside the each nanopore were removed, so that in the first step of the simulation the channel was completely dry. 1 M NaCl was added to the resulting systems. A membrane without any nanopore inserted, of the same dimensions, was also simulated to provide a control. In this way, a total of 6 systems were prepared. The initial size of the unit cell in each case was equal to $15.1 \times 15.2 \times 6.9 \text{ nm}^3$ and contained ~550 lipids, ~1000 cations ~1000 anions and ~18000 water molecules.

Simulations were performed with the GROMACS 4.6⁶⁴ (www.gromacs.org) package. Each system were partially optimized, thermalized, and equilibrated, followed by unrestrained simulations for 30 ns (time step = 2 fs). The constant pressure and temperature NPT ensemble was employed with a pressure of 1 bar controlled using a semi-isotropic Parrinello–Rahman barostat,⁶⁵ and a temperature of 300 K imposed by a V-rescale thermostat (*i.e.* temperature coupling using velocity rescaling with a stochastic term).⁶⁶ The LINCS⁶⁴ algorithm was employed. The Particle Mesh Ewald method⁶⁷ coupled to periodic boundary conditions was used to treat the long-range electrostatics using a direct-space cutoff of 1.0 nm and a grid spacing of 0.12 nm. Van der Waals interactions were computed using a cutoff of 1.0 nm.

Analysis Density maps, radial distribution functions, mass density profiles and bilayer thicknesses were obtained using GROMACS tools. The plots showing the projection of the lipid-to-tail vectors on the membrane plane averaged over the last 20 ns, the displacement distributions and the diffusion constants were determined using locally written code. For the calculation of the lipid-to-tail vectors the XY plane was divided into $2 \times 2 \text{ Å}$ adjacent grids. Lipids were assigned to a given grid when it contains the coordinates of the corresponding phosphorus atom. This assignment was performed for each frame over the last 20 ns of the trajectory. The coordinates of all the phosphorus atoms included at any time within a given grid, together with the projection over the XY plane of the vectors joining that P-atom with the end of each lipid tail, were averaged. The calculations were separately plotted for the two leaflets and also for each lipid tail.

In order to quantify the displacements and diffusion constants as a function of the distance to each channel, the lipids were distributed over concentric 2 Å wide shells of increasing radius around the corresponding nanopore. The minimum distance between the lipid P-atoms and the macromolecule was employed to classify the DOPC molecules into shells for each frame over the trajectory. The projection in the XY plane of the distance to which the lipid P-atom moved over time periods (Δt) of 0.1, 0.5, 1, 2, 5 and 10 ns, regardless it is in a different shell after this time, is taken as the individual lateral displacement of that molecule. Upon repeating the process for all the lipids over the last 20 ns of the trajectory, the mean lateral displacement distributions (MLD) were determined for each shell and time period. It is worth mentioning that the movement of the center of mass of the whole system (the lipid bilayer and the nanopore) has to be removed in order to perform this calculation. In contrast, the nanopore structure should not be fitted or centered throughout the trajectory since this manipulation would introduce an artificial displacement of the lipids that would be more important as the distance to the channel increases. Another artificial source of D increase would be the imperfect correction of lipid movements beyond the periodic boundaries of the simulation box. This error would produce extremely large lipid displacements. As described by Niemelä et al.,⁴⁶ diffusion constants were obtained from the application of the two-dimensional random walk equation [1] to the MSD distributions of the lipid P-atoms, determined as described above.

$$P(r, \Delta t) = r / (2D\Delta t) \exp[-r^2 / (4D\Delta t)] \quad [1]$$

where r is the lateral displacement and D is the lateral diffusion coefficient. The fitting was performed with our own code using a modified Newton–Raphson routine to facilitate the convergence to the minimum, as described in a previous paper.⁶⁸ The employment of this method, instead of the classical least-squares fitting of the mean square displacement to a straight line to obtain the D values from the Einstein relation, was chosen because the corresponding results do not depend upon the fitting interval.

Molecular graphic images were prepared using visual Molecular Dynamics (VMD).⁶⁹

ACKNOWLEDGMENTS

We are grateful for funding from the Spanish Ministry of Science and Innovation MICINN and the ERDF (CTQ2013-43264-R, MAT2011-25501) and the Xunta de Galicia and the ERDF (GPC2013-039 and EM 2012/117). This work was also supported by the Spanish Ministry of Education (Programa de movilidad José Castillejo 2010) and Xunta de Galicia (Programa postdoctoral Ángeles Alvariño 2008-2011). We also thank to the COST CM1306 European Action. All calculations were carried out at the Barcelona Supercomputer Center (BSC-RES), on the Centro de Supercomputación de Galicia (CESGA) and on the UK National Grid Service. Research in MSPS's group is supported by the BBSRC, the Leverhulme Foundation, and the Wellcome Trust.

Supporting Information Available: Additional analyses of simulations (lipid density maps, lipid head-to-tail vectors, mean lateral displacement distributions for lipid shells) are available free of charge *via* the Internet at <http://pubs.acs.org>.

REFERENCES:

1. Matile, S.; Jentzsch, A. V.; Montenegro, J.; Fin, A. Recent Synthetic Transport Systems. *Chem. Soc. Rev.* **2011**, *40*, 2453-2474.
2. Garcia-Fandiño, R.; Amorin, M.; Granja, J. R. (2012) Synthesis of Supramolecular Nanotubes, in *Supramolecular Chemistry: From Molecules to Nanomaterials*, John Wiley & Sons, Ltd.
3. Hou, X.; Guo, W.; Jiang, L. Biomimetic Smart Nanopores and Nanochannels. *Chem. Soc. Rev.* **2011**, *40*, 2385-2401.
4. Chiarabelli, C.; Stano, P.; Luisi, P. L. Chemical Synthetic Biology: A Mini-Review. *Frontiers Microbiol.* **2013**, *4*, 285.
5. Geng, J.; Kim, K.; Zhang, J.; Escalada, A.; Tunuguntla, R.; Comolli, L. R.; Allen, F. I.; Shnyrova, A. V.; Cho, K. R.; Munoz, D.; Wang, Y. M.; Grigoropoulos, C. P.; Ajo-Franklin, C. M.; Frolov, V. A.; Noy, A. Stochastic Transport through Carbon Nanotubes in Lipid Bilayers and Live Cell Membranes. *Nature* **2014**, *514*, 612-615.
6. Chapman, R.; Danial, M.; Koh, M. L.; Jolliffe, K. A.; Perrier, S. Design and Properties of Functional Nanotubes from the Self-Assembly of Cyclic Peptide Templates. *Chem. Soc. Rev.* **2012**, *41*, 6023-6041.
7. Hartgerink, J. D.; Clark, T. D.; Ghadiri, M. R. Peptide Nanotubes and Beyond. *Chemistry-a European Journal* **1998**, *4*, 1367-1372.
8. Brea, R. J.; Reiriz, C.; Granja, J. R. Towards Functional Bionanomaterials Based on Self-Assembling Cyclic Peptide Nanotubes. *Chem. Soc. Rev.* **2010**, *39*, 1448-1456.
9. Montenegro, J.; Ghadiri, M. R.; Granja, J. R. Ion Channel Models Based on Self-Assembling Cyclic Peptide Nanotubes. *Acc. Chem. Res.* **2013**, *46*, 2955-2965.
10. Seifert, A.; Goepfrich, K.; Burns, J. R.; Fertig, N.; Keyser, U. F.; Howorka, S. Bilayer-Spanning DNA Nanopores with Voltage-Switching between Open and Closed State. *ACS Nano* **2015**, *9*, 1117-1126.
11. Chen, X.; Weber, I.; Harrison, R. W. Hydration Water and Bulk Water in Proteins Have Distinct Properties in Radial Distributions Calculated from 105 Atomic Resolution Crystal Structures. *J. Phys. Chem. B* **2008**, *112*, 12073-12080.

12. Atilgan, C.; Aykut, A. O.; Atilgan, A. R. How a Vicinal Layer of Solvent Modulates the Dynamics of Proteins. *Biophys. J.* **2008**, *94*, 79-89.
13. Nakasako, M. Water-Protein Interactions from High-Resolution Protein Crystallography. *Phil. Trans. Roy. Soc. London B* **2004**, *359*, 1191-1204.
14. Raschke, T. M. Water Structure and Interactions with Protein Surfaces. *Curr. Opin. Struct. Biol.* **2006**, *16*, 152-159.
15. Lee, A. G. Lipid-Protein Interactions in Biological Membranes: A Structural Perspective. *Biochim. Biophys. Acta* **2003**, *1612*, 1-40.
16. Contreras, F.-X.; Ernst, A. M.; Wieland, F.; Bruegger, B. Specificity of Intramembrane Protein-Lipid Interactions. *Cold Spring Harbor Perspect. Biol.* **2011**, *3*, a004705.
17. Smith, A. W. Lipid-Protein Interactions in Biological Membranes: A Dynamic Perspective. *Biochim. Biophys. Acta* **2012**, *1818*, 172-177.
18. Lindahl, E.; Sansom, M. S. P. Membrane Proteins: Molecular Dynamics Simulations. *Curr. Opin. Struct. Biol.* **2008**, *18*, 425-431.
19. Biggin, P. C.; Bond, P. J. Molecular Dynamics Simulations of Membrane Proteins. *Methods in molecular biology (Clifton, N.J.)* **2015**, *1215*, 91-108.
20. Wallace, E. J.; Sansom, M. S. P. (2010) Molecular Dynamics Studies of the Interactions between Carbon Nanotubes and Biomembranes, in *Molecular Simulations and Biomembranes: From Biophysics to Function* (Sansom, M. S. P., and Biggin, P. C., Eds.) pp 287-305.
21. Makarucha, A. J.; Todorova, N.; Yarovsky, I. Nanomaterials in Biological Environment: A Review of Computer Modelling Studies. *Eur. Biophys. J.* **2011**, *40*, 103-115.
22. Goose, J. E.; Sansom, M. S. P. Reduced Lateral Mobility of Lipids and Proteins in Crowded Membranes. *PLoS Comp. Biol.* **2013**, *9*, e1003033.
23. Chiu, S. W.; Subramaniam, S.; Jakobsson, E. Simulation Study of a Gramicidin/Lipid Bilayer System in Excess Water and Lipid. I. Structure of the Molecular Complex. *Biophys. J.* **1999**, *76*, 1929-1938.
24. Schmidt, D.; MacKinnon, R. Voltage-Dependent K⁺ Channel Gating and Voltage Sensor Toxin Sensitivity Depend on the Mechanical State of the Lipid Membrane. *Proc. Natl. Acad. Sci. USA* **2008**, *105*, 19276-19281.
25. Krepiy, D.; Mihailescu, M.; Freitas, J. A.; Schow, E. V.; Worcester, D. L.; Gawrisch, K.; Tobias, D. J.; White, S. H.; Swartz, K. J. Structure and Hydration

- of Membranes Embedded with Voltage-Sensing Domains. *Nature* **2009**, *462*, 473-479.
26. Krepiy, D.; Gawrisch, K.; Swartz, K. J. Structural Interactions between Lipids, Water and S1-S4 Voltage-Sensing Domains. *J. Molec. Biol.* **2012**, *423*, 632-647.
 27. Lelimosin, M.; Sansom, M. S. P. Membrane Perturbation by Carbon Nanotube Insertion: Pathways to Internalization. *Small* **2013**, *9*, 3639-3646.
 28. Kostarelos, K. The Long and Short of Carbon Nanotube Toxicity. *Nature Biotech.* **2008**, *26*, 774-776.
 29. Garcia-Fandiño, R.; Sansom, M. S. P. Designing Biomimetic Pores Based on Carbon Nanotubes. *Proc. Natl. Acad. Sci. USA* **2012**, *109*, 6939-6944.
 30. Kostarelos, K.; Bianco, A.; Prato, M. Promises, Facts and Challenges for Carbon Nanotubes in Imaging and Therapeutics. *Nature Nanotech.* **2009**, *4*, 627-633.
 31. Shityakov, S.; Dandekar, T. Molecular Dynamics Simulation of Popc and Pope Lipid Membrane Bilayers Enforced by an Intercalated Single-Wall Carbon Nanotube. *Nano* **2011**, *6*, 19-29.
 32. Ghadiri, M. R.; Granja, J. R.; Milligan, R. A.; McRee, D. E.; Khazanovich, N. Self-Assembling Organic Nanotubes Based on a Cyclic Peptide Architecture. *Nature* **1993**, *366*, 324-327.
 33. Sanchez-Ouesada, J.; Isler, M. P.; Ghadiri, M. R. Modulating Ion Channel Properties of Transmembrane Peptide Nanotubes through Heteromeric Supramolecular Assemblies. *J. Amer. Chem. Soc.* **2002**, *124*, 10004-10005.
 34. Kim, H. S.; Hartgerink, J. D.; Ghadiri, M. R. Oriented Self-Assembly of Cyclic Peptide Nanotubes in Lipid Membranes. *J. Amer. Chem. Soc.* **1998**, *120*, 4417-4424.
 35. Bong, D. T.; Clark, T. D.; Granja, J. R.; Ghadiri, M. R. Self-Assembling Organic Nanotubes. *Angewandte Chemie Int. Edn.* **2001**, *40*, 988-1011.
 36. Garcia-Fandiño, R.; Amorin, M.; Castedo, L.; Granja, J. R. Transmembrane Ion Transport by Self-Assembling Alpha,Gamma-Peptide Nanotubes. *Chem. Sci.* **2012**, *3*, 3280-3285.
 37. Calvelo, M.; Vazquez, S.; Garcia-Fandino, R. Molecular Dynamics Simulations for Designing Biomimetic Pores Based on Internally Functionalized Self-Assembling Alpha,Gamma-Peptide Nanotubes. *Phys. Chem. Chem. Phys.* **2015**, *17*, 28586-28601.

38. Killian, J. A.; von Heijne, G. How Proteins Adapt to a Membrane-Water Interface. *Trends Biochem. Sci.* **2000**, *25*, 429-434.
39. Trick, J. L.; Wallace, E. J.; Bayley, H.; Sansom, M. S. P. Designing a Hydrophobic Barrier within Biomimetic Nanopores. *ACS Nano* **2014**, *8*, 11268-11279.
40. Richard, C.; Balavoine, F.; Schultz, P.; Ebbesen, T. W.; Mioskowski, C. Supramolecular Self-Assembly of Lipid Derivatives on Carbon Nanotubes. *Science* **2003**, *300*, 775-778.
41. Gapsys, V.; de Groot, B. L.; Briones, R. Computational Analysis of Local Membrane Properties. *J. Comp.-Aided Molec. Design* **2013**, *27*, 845-858.
42. Bohinc, K.; Kralj-Iglic, V.; May, S. Interaction between Two Cylindrical Inclusions in a Symmetric Lipid Bilayer. *J. Chem. Phys.* **2003**, *119*, 7435-7444.
43. Nielsen, S. O.; Ensing, B.; Ortiz, V.; Moore, P. B.; Klein, M. L. Lipid Bilayer Perturbations around a Transmembrane Nanotube: A Coarse Grain Molecular Dynamics Study. *Biophys. J.* **2005**, *88*, 3822-3828.
44. Zimmerli, U.; Koumoutsakos, P. Simulations of Electrophoretic Rna Transport through Transmembrane Carbon Nanotubes. *Biophys. J.* **2008**, *94*, 2546-2557.
45. Yeagle, P. L. (2011) *The Structure of Biological Membranes*, CRC Press.
46. Niemela, P. S.; Miettinen, M. S.; Monticelli, L.; Hammaren, H.; Bjelkmar, P.; Murtola, T.; Lindahl, E.; Vattulainen, I. Membrane Proteins Diffuse as Dynamic Complexes with Lipids. *J. Amer. Chem. Soc.* **2010**, *132*, 7574-+.
47. Striolo, A. The Mechanism of Water Diffusion in Narrow Carbon Nanotubes. *Nano Lett.* **2006**, *6*, 633-639.
48. Farimani, A. B.; Aluru, N. R. Spatial Diffusion of Water in Carbon Nanotubes: From Fickian to Ballistic Motion. *J. Phys. Chem. B* **2011**, *115*, 12145-12149.
49. Vacha, R.; Siu, S. W. I.; Petrov, M.; Bockmann, R. A.; Barucha-Kraszewska, J.; Jurkiewicz, P.; Hof, M.; Berkowitz, M. L.; Jungwirth, P. Effects of Alkali Cations and Halide Anions on the Dopc Lipid Membrane. *J. Phys. Chem. A* **2009**, *113*, 7235-7243.
50. Vacha, R.; Jurkiewicz, P.; Petrov, M.; Berkowitz, M. L.; Bockmann, R. A.; Barucha-Kraszewska, J.; Hof, M.; Jungwirth, P. Mechanism of Interaction of Monovalent Ions with Phosphatidylcholine Lipid Membranes. *J. Phys. Chem. B* **2010**, *114*, 9504-9509.

51. Pan, J. J.; Cheng, X. L.; Monticelli, L.; Heberle, F. A.; Kucerka, N.; Tieleman, D. P.; Katsaras, J. The Molecular Structure of a Phosphatidylserine Bilayer Determined by Scattering and Molecular Dynamics Simulations. *Soft Matter* **2014**, *10*, 3716-3725.
52. Yang, J.; Calero, C.; Bonomi, M.; Marti, J. Specific Ion Binding at Phospholipid Membrane Surfaces. *J. Chem. Theor. Comput.* **2015**, *11*, 4495-4499.
53. Liu, J.; Hopfinger, A. J. Identification of Possible Sources of Nanotoxicity from Carbon Nanotubes Inserted into Membrane Bilayers Using Membrane Interaction Quantitative Structure-Activity Relationship Analysis. *Chem. Res. Toxicol.* **2008**, *21*, 459-466.
54. Stapleton, J. A.; Whitehead, T. A.; Nanda, V. Computational Redesign of the Lipid-Facing Surface of the Outer Membrane Protein Ompa. *Proc. Natl. Acad. Sci. USA* **2015**, *112*, 9632-9637.
55. Brohawn, S. G.; Campbell, E. B.; MacKinnon, R. Physical Mechanism for Gating and Mechano Sensitivity of the Human Traak K⁺ Channel. *Nature* **2014**, *516*, 126-U345.
56. Brohawn, S. G.; Su, Z. W.; MacKinnon, R. Mechanosensitivity Is Mediated Directly by the Lipid Membrane in Traak and Trek1 K⁺ Channels. *Proc. Natl. Acad. Sci. USA* **2014**, *111*, 3614-3619.
57. Pliotas, C.; Dahl, A. C. E.; Rasmussen, T.; Mahendran, K. R.; Smith, T. K.; Marius, P.; Gault, J.; Banda, T.; Rasmussen, A.; Miller, S.; Robinson, C. V.; Bayley, H.; Sansom, M. S. P.; Booth, I. R.; Naismith, J. H. The Role of Lipids in Mechanosensation. *Nature Struct. Mol. Biol.* **2015**, *22*, 991-998.
58. Yoo, J.; Aksimentiev, A. Molecular Dynamics of Membrane-Spanning DNA Channels: Conductance Mechanism, Electro-Osmotic Transport, and Mechanical Gating. *J. Phys. Chem. Lett.* **2015**, *6*, 4680-4687.
59. Wang, J. M.; Wolf, R. M.; Caldwell, J. W.; Kollman, P. A.; Case, D. A. Development and Testing of a General Amber Force Field. *J. Comp. Chem.* **2004**, *25*, 1157-1174.
60. Case, D. A.; Cheatham, T. E.; Darden, T.; Gohlke, H.; Luo, R.; Merz, K. M.; Onufriev, A.; Simmerling, C.; Wang, B.; Woods, R. J. The Amber Biomolecular Simulation Programs. *J. Comp. Chem.* **2005**, *26*, 1668-1688.

61. Joung, I. S.; Cheatham, T. E., III. Determination of Alkali and Halide Monovalent Ion Parameters for Use in Explicitly Solvated Biomolecular Simulations. *J. Phys. Chem. B* **2008**, *112*, 9020-9041.
62. Wang, J.; Wang, W.; Kollman, P. A.; Case, D. A. Automatic Atom Type and Bond Type Perception in Molecular Mechanical Calculations. *J. Molec. Graph. Model.* **2006**, *25*, 247-260.
63. Siu, S. W. I.; Vacha, R.; Jungwirth, P.; Boeckmann, R. A. Biomolecular Simulations of Membranes: Physical Properties from Different Force Fields. *J. Chem. Phys.* **2008**, *128*.
64. Hess, B.; Bekker, H.; Berendsen, H. J. C.; Fraaije, J. Lincs: A Linear Constraint Solver for Molecular Simulations. *J. Comp. Chem.* **1997**, *18*, 1463-1472.
65. Parrinello, M.; Rahman, A. Polymorphic Transitions in Single-Crystals - a New Molecular-Dynamics Method. *J. Appl. Phys.* **1981**, *52*, 7182-7190.
66. Bussi, G.; Donadio, D.; Parrinello, M. Canonical Sampling through Velocity Rescaling. *J. Chem. Phys.* **2007**, *126*.
67. Essmann, U.; Perera, L.; Berkowitz, M. L.; Darden, T.; Lee, H.; Pedersen, L. G. A Smooth Particle Mesh Ewald Method. *J. Chem. Phys.* **1995**, *103*, 8577-8593.
68. Piggot, T. J.; Pineiro, A.; Khalid, S. Molecular Dynamics Simulations of Phosphatidylcholine Membranes: A Comparative Force Field Study. *J. Chem. Theor. Comp.* **2012**, *8*, 4593-4609.
69. Humphrey, W.; Dalke, A.; Schulten, K. Vmd: Visual Molecular Dynamics. *J. Molec. Graphics Mod.* **1996**, *14*, 33-38.

Figures

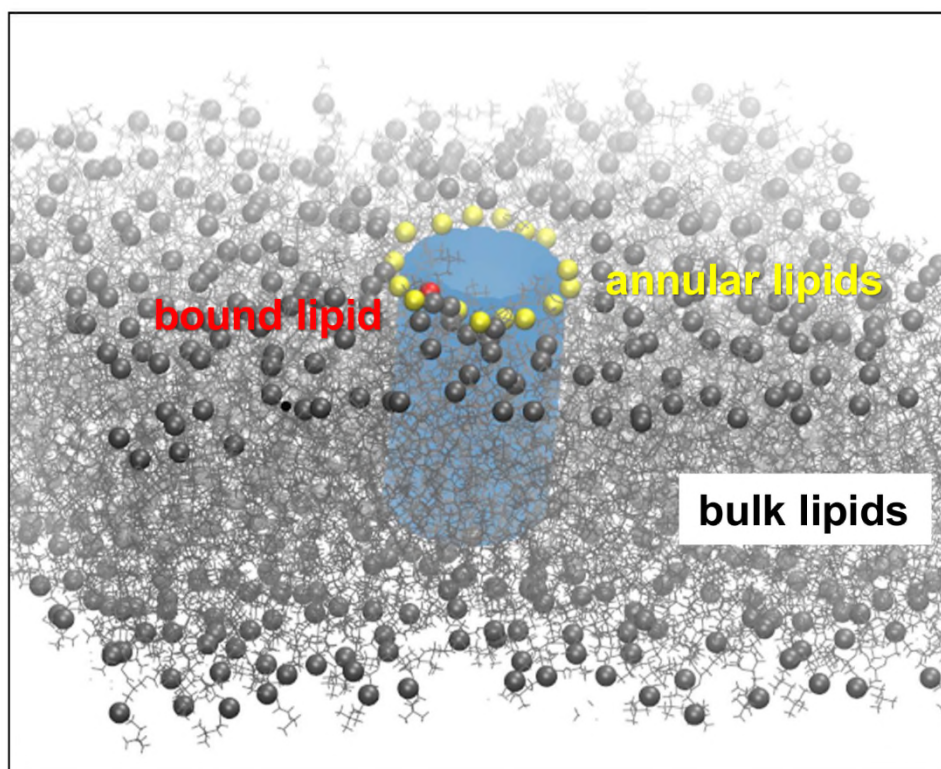


Figure 1: Representation of “bulk” lipids (grey), annular lipids (yellow) around a nanopore model and bound lipids (red), residing at the interface between different subunits or domains of the nanopore.

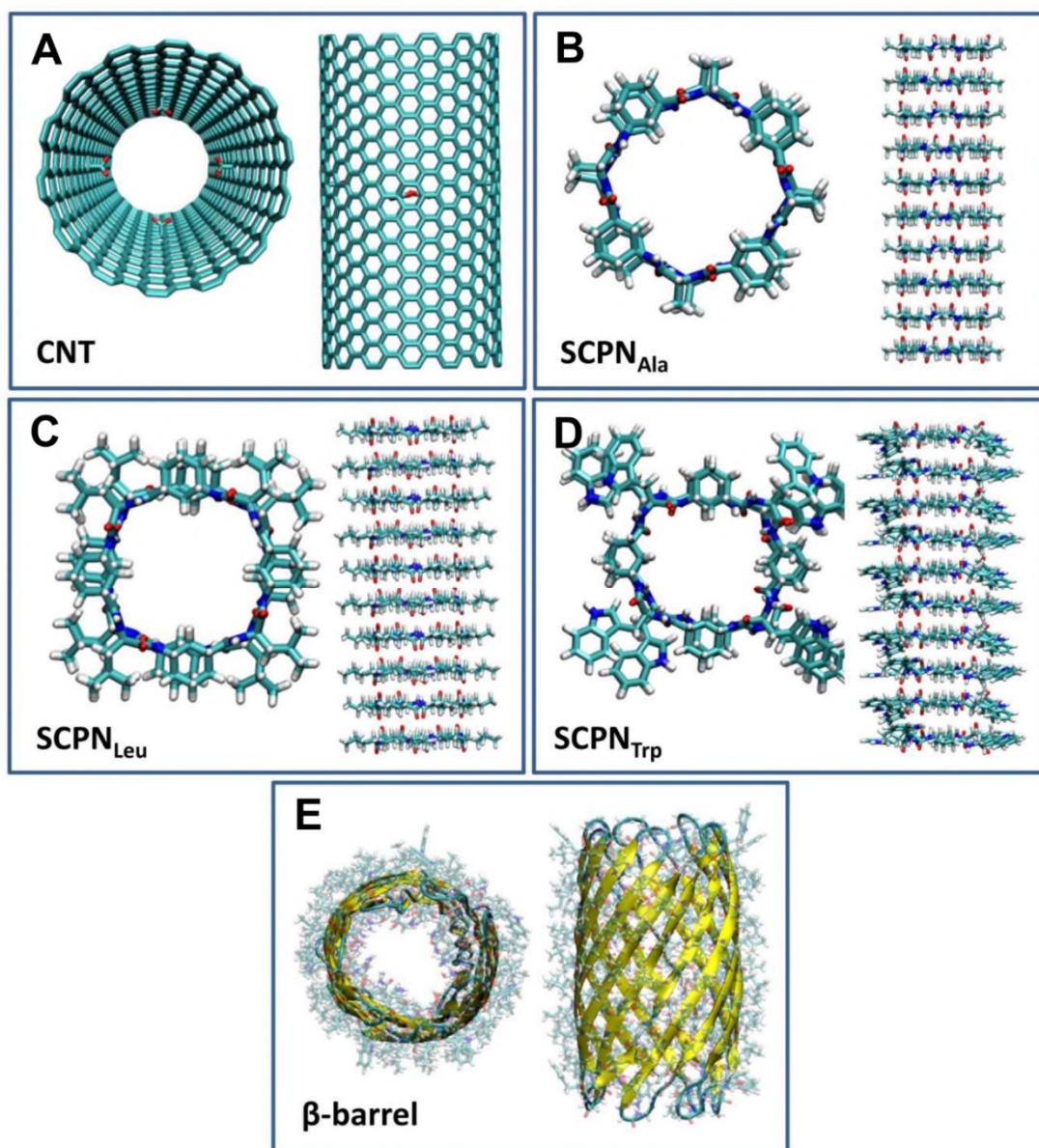


Figure 2: Structure of the systems employed in this study: **A** a (single walled) carbon nanotube (CNT), **B,C,D** three SCPNs combining γ -residues with Ala, Leu or Trp (SCPN_{Ala}, SCPN_{Leu} and SCPN_{Trp} respectively) and **E** a minimalist model for biomimetic β -barrel nanopores (β -barrel).

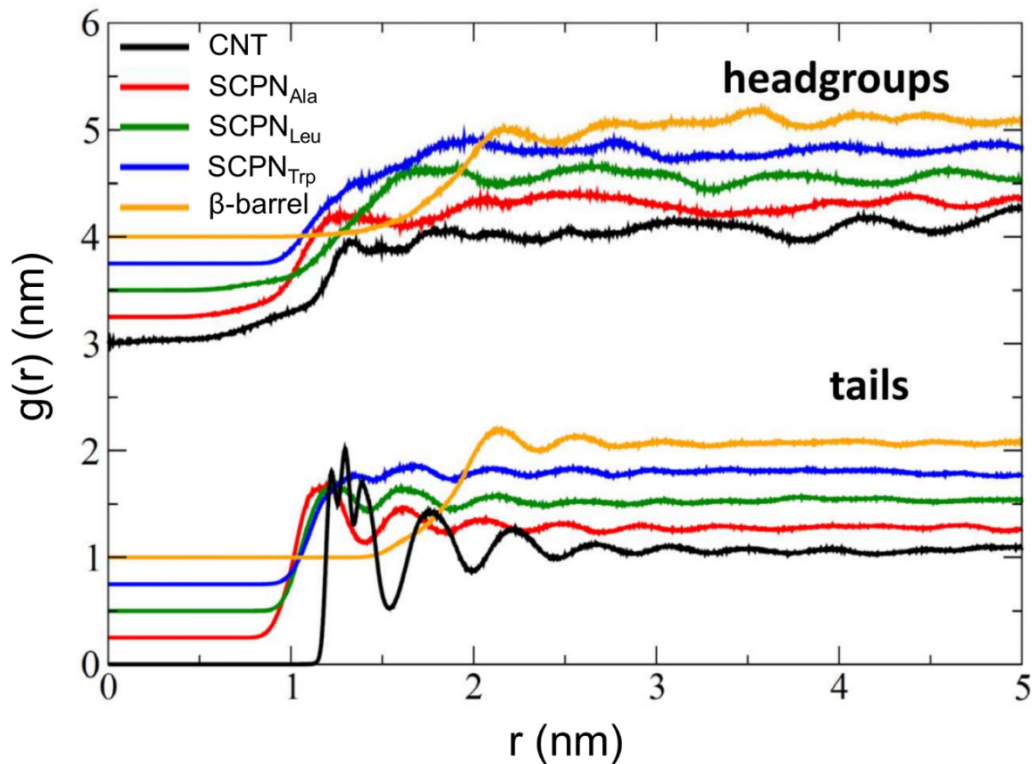


Figure 3: Radial distribution function (RDF; $g(r)$) of the headgroups (upper panel) and tails (lower panel) of DOPC lipid molecules around the nanopores studied in this work, averaged over the last 20 ns of the MD simulations: **CNT** (black), **SCPN_{Ala}** (red), **SCPN_{Leu}** (green), **SCPN_{Trp}** (blue) and **β-barrel** (orange). The $g(r)$ curves were purposely displaced vertically relative to one another to make them easier to compare.

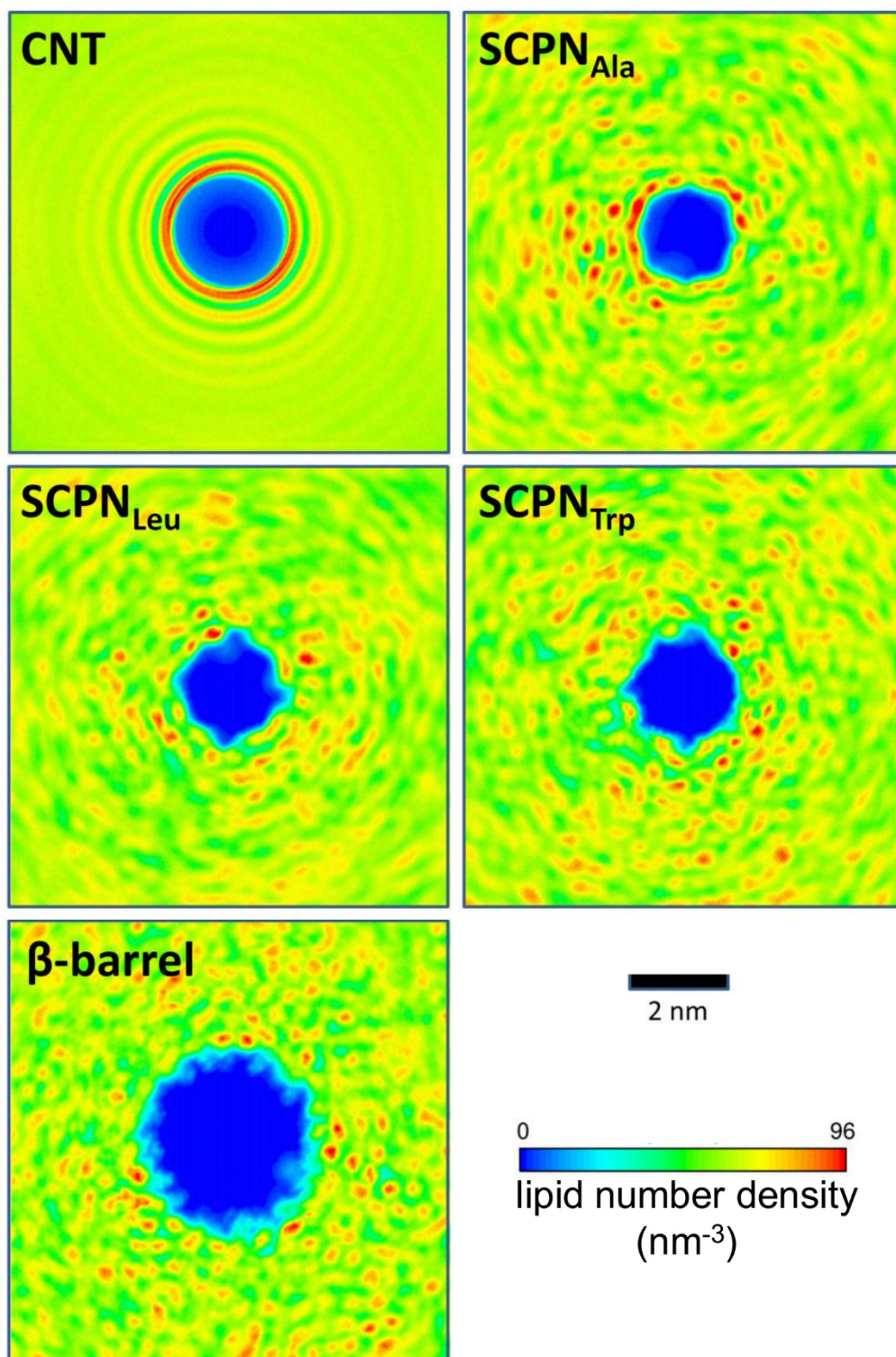


Figure 4: 2D-density maps in the plane of the bilayer (XY) for lipids along the MD simulation of each nanopore in a POPC bilayer, averaged over the last 20 ns of the simulations. (An analogous analysis for the pure POPC bilayer is presented in SI Figure S1).

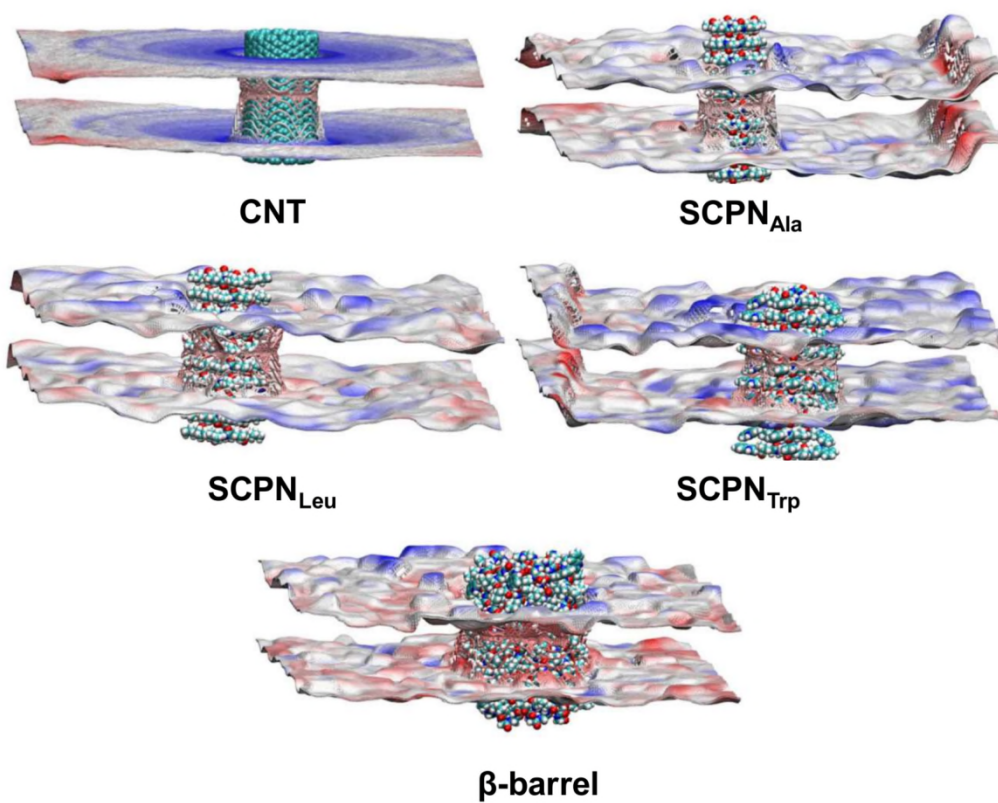


Figure 5: Local membrane thickness for the simulated systems, obtained with the g_lomepro⁴¹ tool. The thickness increases as a red-white-blue color gradient. An analogous analysis for a pure POPC bilayer is presented in SI Figure S1).

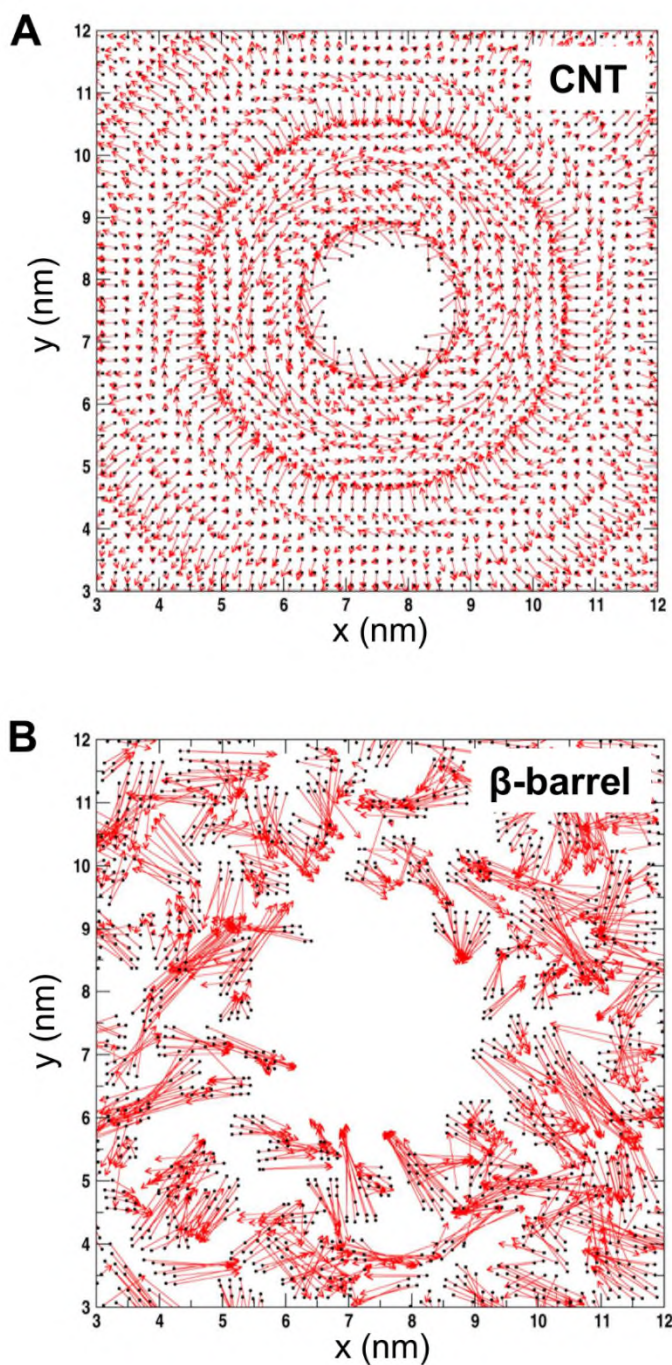


Figure 6: Average distribution of lipid head phosphorous atoms and projection of lipid head-to-tail vectors on the membrane plane, averaged over the last 20 ns of the **A CNT** or the **B β -barrel** (B) trajectory for a network of 2x2 Å grids. Only the contribution of the *sn1* tails of a single leaflet is shown in this plot. A complete analysis of both tails for the two leaflets and for all the studied systems is shown in SI Figures S4-S8.

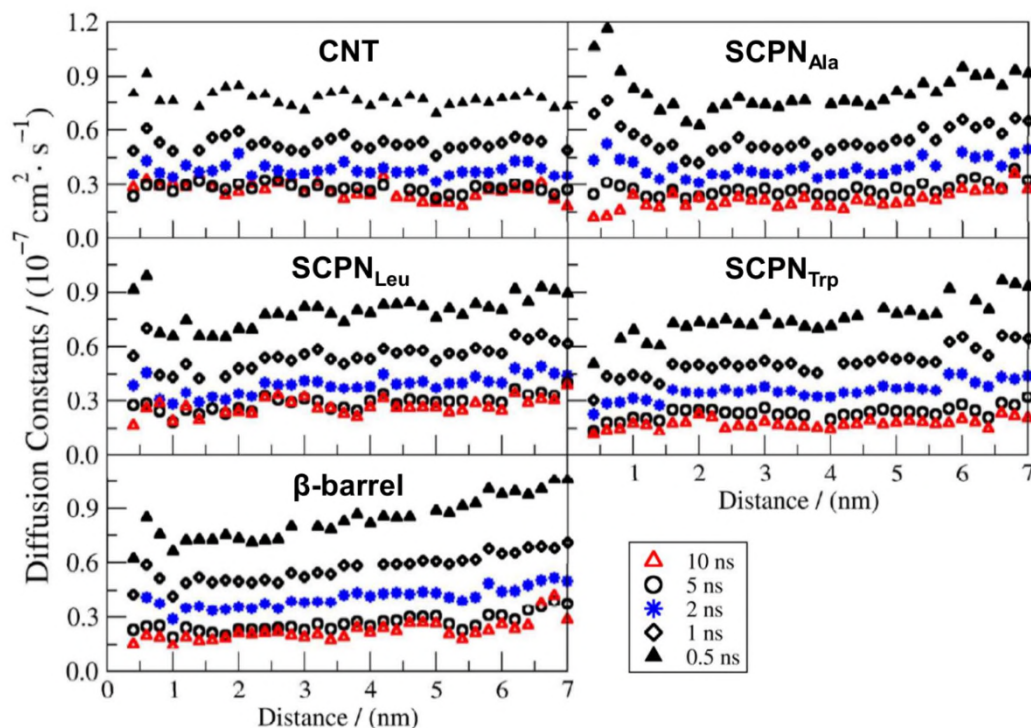


Figure 7: Diffusion constants (D) as a function of the minimum distance to the macromolecule, obtained from the application of the two-dimensional random walk equation [1] to the mean lateral displacement (MLD) distributions over the last 20 ns of the trajectory. The Δt values employed to generate the displacement distributions are indicated within the plots. The same graphics including also the results at $\Delta t = 0.1$ ns are indicated in SI Figure S12.

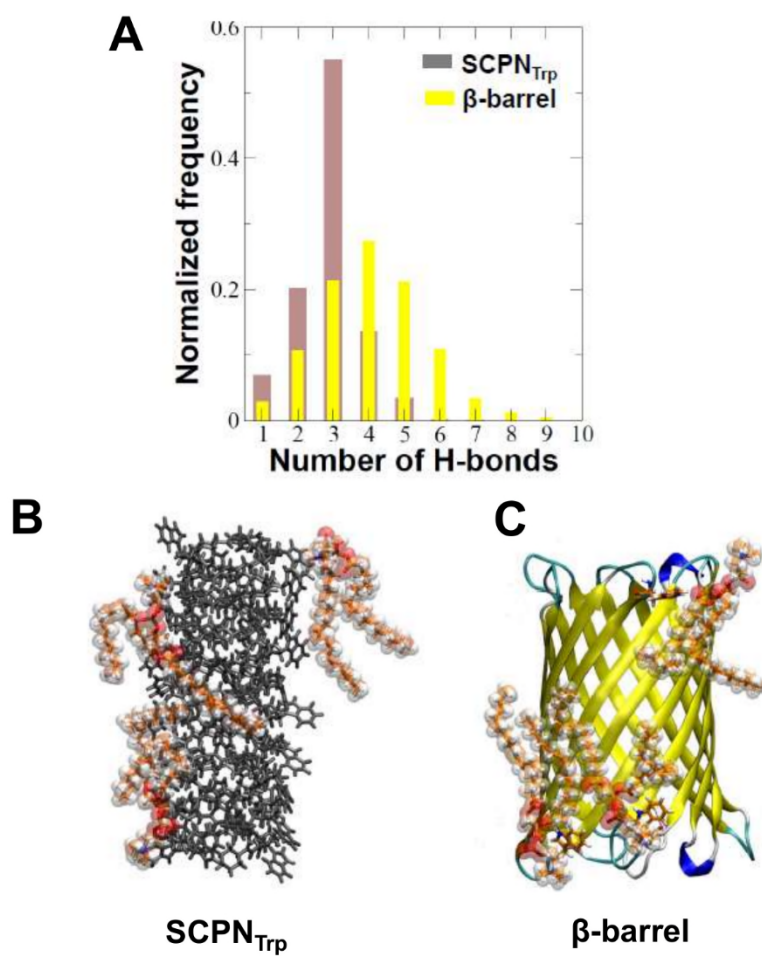


Figure 8: **A** Histogram with the number of hydrogen bonds between SCPN_{Trp}, and β -barrel and the lipids along the trajectory (top left). Detail of selected lipids H-bonded to **B** SCPN_{Trp}, and **C** β -barrel are shown.

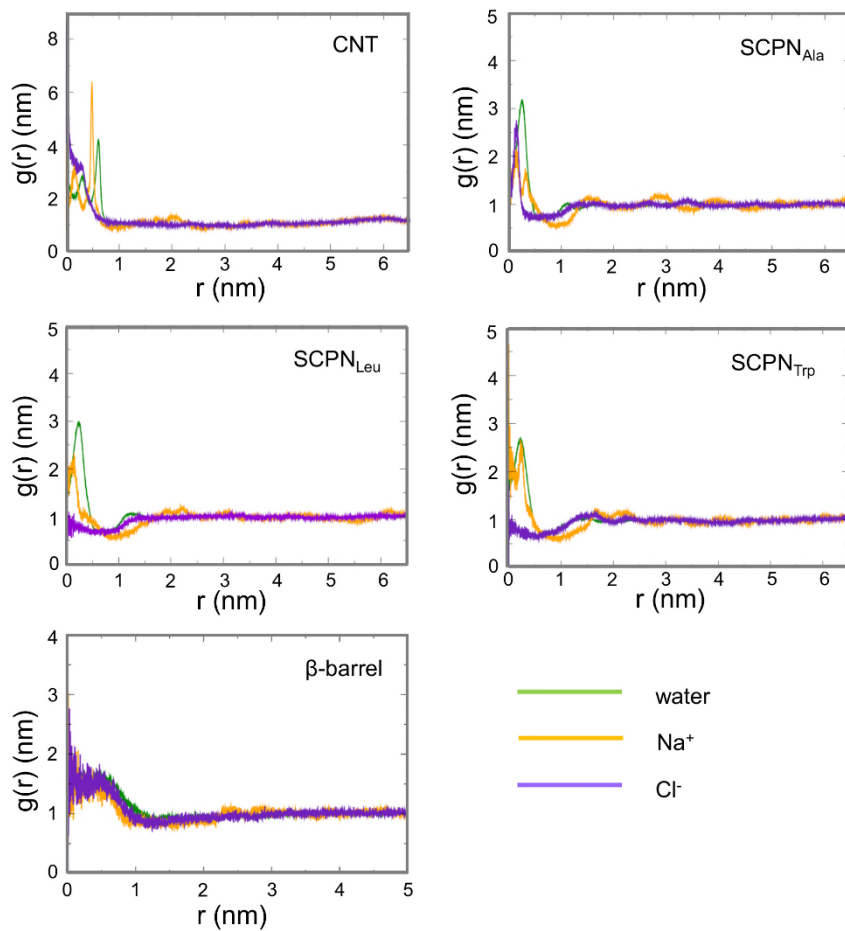


Figure 9: Radial distribution functions (in the bilayer plane, XY) of water (green lines), sodium ions (orange), and chloride ions (purple), as a function of distance from the centre of the nanotubes.

Table of Contents Graphic

